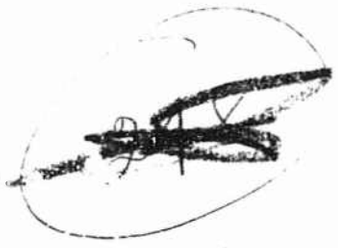

(1)

(6) PERFORMANCE ANALYSIS OF THE 'HORTEN IV' FLYING WING (5)

by

(10) Dezso Gyorgyfalvy.

(11) 1960,

(12) 35 p.

(21) Presented at the 8th Congress of ~~the~~ the Organisation Scientifique et Technique Internationale du Vol a Voile, Jun 60, Cologne, ~~Western~~ Germany.

~~The Aerophysics Department~~
~~Mississippi State University~~

(243 425) Clark

ACKNOWLEDGEMENTS

This work was done under the sponsorship of the United States Army Transportation Command and Office of Naval Research. Dr. August Raspet, Head of the Aerophysics Department took the initiative in this study and gave full support and inspiration. A special appreciation is due to Mr. Rudolf Opitz, who saved the Horten IV from deterioration, rebuilt and flew it with remarkable success in the U. S. National Contest of 1951, as well as in the early flight tests at Mississippi State University, then introduced the author to flying the plane and gave over much of his vast experience on flying wings. Besides, the author wishes to express his gratitude to his colleagues, Mrs. Sue Parker, Mrs. Wren Bridges, Mrs. Lucy Inkster, Mr. Melvin Swartzberg, Mr. Benny Boggs, and Mr. Steve Marton, who participated and assisted in this research, particularly to Mrs. Elwanda Smith, who gave essential help in the computation and data reduction. The author is also indebted to Mr. T. W. Feistel for his constructive criticism in the preparation of the manuscript.

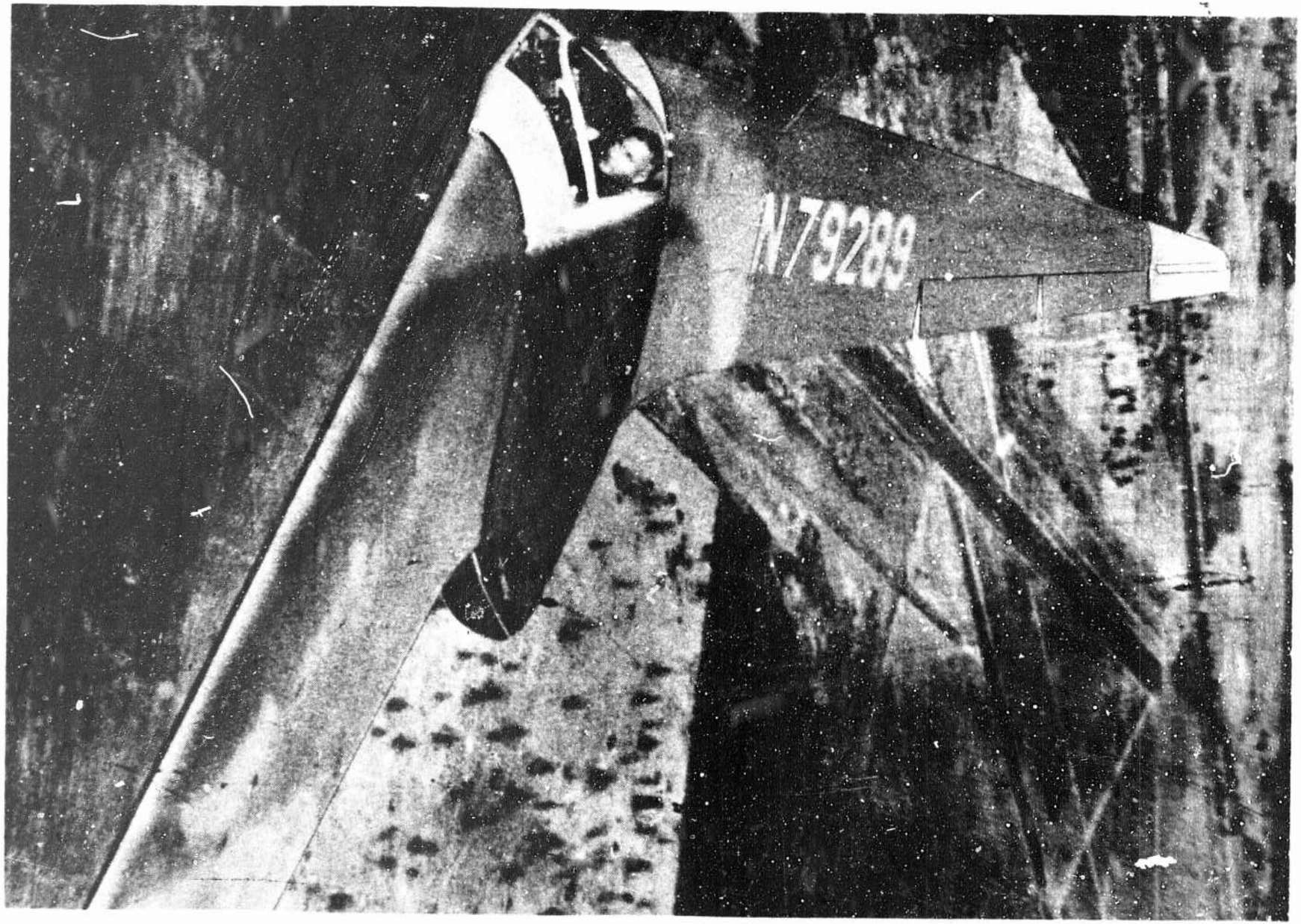
N79289

SYMBOLS

A. C.		aerodynamic center
b	m	wingspan
c	m	chord length
C. G.	-	center of gravity
C_D	-	total drag coefficient
C_L	-	resultant lift coefficient
c_l	-	section lift coefficient
C_{D_p}	-	resultant profile drag coefficient
c_{d_p}	-	section profile drag coefficient
C_{D_i}	-	induced drag coefficient
e	-	span efficiency
Re	-	Reynolds number
S	m^2	wing area
V	km/h	calibrated airspeed
W	kg	gross weight
w	m/sec	sinking speed
$\bar{y}$	m	distance perpendicular to the symmetry axis
α	deg.	angle of attack
δ	-	factor of induced drag increment
δ_e	deg.	elevon deflection angle
ε	-	gliding ratio
γ	deg.	glide path angle
θ	deg.	pitch angle
λ	-	geometric aspect ratio b^2/S
λ_{eff}	-	effective aspect ratio

MAIN DIMENSIONS OF THE HORTEN IV *

Span	20	m
Wing area	18.8	m^2
Aspect ratio	21.3	
Dihedral	5	degrees
Sweep-back (1/4 chord line)	17	degrees
Twist	7.1	degrees
Wing root chord	1.55	m
Wing tip chord	0.28	m
Taper ratio	5.55	
Airfoil sections	Reflexed, individual design	
Total area of elevon surfaces	3.16	m^2
Ratio of the elevon surfaces to the total wing area	16.8	%
Total wetted area	41	m^2
Ratio of the wetted area to the total wing area	2.18	
Empty weight (present condition)	266	kg
Gross weight (recent flight tests)	366	kg
Wing loading " " "	19.5	kg/m^2

* Most of the data are taken from Reference 1.

PERFORMANCE ANALYSIS OF THE "HORTEN IV" FLYING WING

Introduction

It has been recognized from the beginning of the development of the sailplane that the key to performance improvement was in drag reduction. It has been also known that the total drag consisted of three major components: induced, profile, and parasite drag. The development started first in reducing the parasite drag by elimination of struts, wires, open cockpit, etc. Then, it continued in decreasing the induced drag by using high aspect ratio. The third stage of the development is going on at the present time, when the major effort is concentrated on lowering the profile or friction drag, since the possibilities of induced and parasite drag reduction are nearly exhausted.

During the second stage of development, the continuous aspiration for lower and lower drag led to the idea of the flying wing design. This offered the complete elimination of the parasite drag in addition to lighter weight and lower cost. But, at the same time, numerous problems of stability and control were to be overcome. These difficulties discouraged most of the designers, but the Horten brothers took up the problem with great determination and basically solved it. It is most remarkable that the fourth of their models, the Horten IV, was already better, or at least equivalent in performance to those of conventional design, which were developed with all the experience gained through dozens of previous models. This successful development, however, was interrupted by the war, and the last two models of the line, the Horten IV b and Horten VI, remained unevaluated.

Since the war, the emphasis in sailplane development has been concentrated mostly on the profile or friction drag reduction of conventional types. The adoption of laminar airfoils and new technology brought significant progress, and the seemingly ultimate gliding ratio of 40 to 1 has been reached. But, in this state of development when

the heavy effort is necessary to eliminate one or two thousandths from the profile drag coefficient, the presence of the parasite drag due to the fuselage and tail becomes more and more annoying, and the idea of the flying wing configuration comes into prominence again.

For this reason, as a part of the sailplane research program conducted by the Aerophysics Department of Mississippi State University, an investigation was projected into flying wing sailplanes, and a Horten IV was chosen for that purpose as the most advanced design of its class.

Preliminary performance measurements of the Horten IV were made by the DFS in comparison flight with the D-30 Cirrus in 1943, and reported by Hans Zacher.[2]

It was pointed out that, although the Horten IV was one of the best performing sailplanes of that time, the actual performance was well below that expected.

The basic aim of our research was to find out why the estimated performance could not be achieved and whether or not the factors causing the lower performance are inherent in the flying wing design.

Preliminary flight tests at Mississippi State University showed even lower performance than reported by Zacher. Since the plane was not in good condition at that time, it was decided to overhaul it, improving the wing surfaces as much as possible and making some modifications on the center section, such as streamlined housing for the nose skid and improved canopy contour. Finally, the prospected flight tests were conducted in the fall of 1959, and the results of the evaluation are presented here.

Results of Recent Performance Measurements

Figure 1 shows the performance curves. The test points of several flights are indicated by different symbols. The points were weighed according to the customary method,[3] and those of full weight have filled symbol. In addition to our measurements, the former DFS test results are also indicated. They are reduced to $W = 366$ kg., the gross weight of the recent tests.

The best gliding ratio of the Horten IV was expected to be . 37. The flight tests, however, indicated considerably lower performance. Nevertheless, there is some difference between the flight test data also. While the drag polars in Figure 2 almost coincide at low lift coefficients, the deviation between them becomes larger and larger as the lift coefficient increases. In other words, the slope of the linearized drag polar is steeper according to the DFS measurements, which means better span efficiency. It should be noted, however, that the span efficiency is affected by the C. G. position, and it is not given for the DFS test. If the C. G. was located considerably farther back in the DFS test, or if the two planes were not the same, the disagreement is understandable.

The most important performance and aerodynamic data are summarized in Table 1.

Three features of the aerodynamic characteristics are most remarkable.

1. The minimum drag coefficient, $C_{D_{min}} = 0.0125$, is barely lower than that of a good conventional design of that time in spite of the elimination of the fuselage and tail. $C_{D_{min}}$ was 0.0135 for the D-30 "Cirrus," and 0.015 for the DFS "Reiher,"[4]

2. The drag rapidly increases with the lift coefficient, that is, the slope of the linearized drag polar is extremely shallow, which means poor span efficiency or low effective aspect ratio.

3. The maximum lift coefficient, $C_{L_{max}} = 1.125$, is relatively low also.

Analysis of the Drag Components

The performance measurements represented only the first step in our investigation. As mentioned before, the basic aim was to find out the reasons for the unusual behavior and to make clear the interaction of the several influential factors. For this a detailed study of the individual drag components was necessary, or in other words, the drag polar was to be broken down into its elements.

The Profile Drag

The profile drag was measured at several places along the span by means of an integrating wake rake. The method is described in Reference 5. The measured profile drag polars, Figure 3, have the following features: Going outwards along the span, the drag increases considerably. This is partly due to the decrease of Reynolds number, but most likely is due to the uncleannes of the airfoil caused by elevon surfaces, dive brakes, and drag rudders.

In the case of the innermost test section, the minimum profile drag coefficient $c_{d_{p\,min}} = 0.009$. Then the drag gradually increases at the higher lift coefficients, and amounts to $c_{d_p} = 0.015$ at $C_L = 1.125$.

Although, in view of the present state of the art, an airfoil of such a high drag is considered very unfavorable, it was not worse than other contemporary airfoils.[4, 6]

For the rest of the test sections, the airfoils are not clean due to dive brakes and control surfaces. At the second and third test section there is a rapid drag increase at high lift coefficients. This is generated by turbulent separation, which occurs on that part of the wing as an initiation of the stall.

For the fourth test section, the rate of drag increase with lift coefficient is much greater than for the inner sections, but there is no rapid growth in drag at high lift coefficients. This is because the center elevon has large negative deflection which results in higher drag at moderate lift coefficients, but does not allow separation at the high lift coefficients.

The outermost test section has approximately two and one-half times higher drag than the innermost one. Numerous factors, such as contour and surface imperfections, drag rudder, low Reynolds number, large control surface-chord ratio, etc., contribute to develop this extremely high drag at the wing tip. It is peculiar that the minimum drag occurs at $C_L = 0.4$, and below that the drag increases again. The probable reason for this is the discontinuity in profile contour which causes the flow to separate from the drag rudder when the elevon

has zero or positive deflection, while the outhanging nose of the Frise-type elevon creates rapidly increasing drag at high lift coefficients when large negative deflection is applied.

Based on the sectional profile drag measurements, the spanwise profile drag distribution and resultant profile drag polar were determined. Figure 4 shows the local profile drag coefficients along the span. These curves, multiplied by the local chord length, represent the effective drag distribution and the resultant profile drag is calculated as:

$$C_{D_p} = \frac{2}{S}\int_0^{b/2} (c_{d_p} c)\, dy$$

The results are given below.

RESULTANT PROFILE DRAG COEFFICIENTS

C_L	0.2	0.4	0.6	0.8	1.0	1.05	1.125
C_{D_p}	0.0115	0.0120	0.0132	0.0151	0.0179	0.0208	0.0223

Induced Drag

The induced drag coefficient is defined as:

$$C_{D_i} = \frac{C_L^2}{\pi \lambda}(1+\delta)$$

where the factor δ represents the induced drag increment due to the deviation of spanwise lift distribution from elliptic, which would give the minimum induced drag. It is customary to express the induced drag coefficient also as:

$$C_{D_i} = \frac{C_L^2}{\pi \lambda_{eff}}$$

that is, to consider the induced drag increment as a consequence of decreased effective aspect ratio, where

$$\lambda_{eff} = e\lambda .$$

and e , the span efficiency, is defined as

$$e = \frac{C_{Di\,ell}}{C_{Di}} = \frac{1}{1+\delta}$$

The low span efficiency of the Horten IV propounded that the induced drag increment might be very high because of the intense twist and control deflection. Therefore, a detailed calculation was carried out concerning the spanwise lift distribution and actual induced drag.

The factor δ is determined by the spanwise lift distribution which is affected mainly by the taper, sweep, twist, and control deflection. The spanwise lift distribution was calculated according to O. Schrenk's approximate method, supplemented by Weissinger's correction for sweep.[7, 8, 9]

The most unusual among the influencing factors considered is the control deflection. In low speed flight the center and outboard elevons are deflected up as much as 15 degrees, which results in a considerably decreased effective local angle of attack or lift coefficient.

The elevator deflection angles are shown as a function of the lift coefficient in Figure 5. This was obtained by collating the curves $\delta_E^* = f(C_L)$ and $\delta_E^\circ = f(\delta^*)$, where δ^* represents the displacement of the control grip and δ° is the control surface deflection in degrees.

According to theory, a small control deflection results in a change of effective angle of attack defined by the control power derivative $\frac{d\alpha}{d\delta_E}$, that is,

$$\Delta\alpha = \frac{d\alpha}{d\delta}\,\delta_E$$

This change in angle of attack due to control deflection was considered as additional twist, and the resultant lift distribution calculated accordingly.

Figure 6 illustrates the deviation of the lift distribution from the elliptic for the wing with basic twist only, and for that with control deflection included. Two examples are presented: $C_L = 1.00$, and

$C_L = 0.25$. As can be seen, at high lift coefficient, the large negative control deflection greatly increases the deviation of the ($c_l c$) curve from the elliptic, while the basic twist results in minor difference.

However, at low lift coefficient, the control deflection, being positive, decreases the effective twist and brings the resultant lift distribution closer to the elliptic than it is for the wing of basic twist.

The induced drag increment, δ, was calculated by the formula: (Reference 10)

$$1 + \delta = \frac{\sum_n (n a_n^2)}{a_1^2}$$

where a_1 and a_n are the Fourier coefficients of the ($c_l c$) lift distribution curves.

The results are summarized in Figure 7, where δ is plotted versus C_L. The effect of taper, sweep, twist, and control deflection can be delineated clearly. The extreme taper causes an induced drag increment of about 2.5 per cent, as compared to an elliptical planform. The sweep, by shifting the load towards the tips, counteracts the taper and reduces δ to about 1.5 per cent. Contrary to the former two factors, in which cases δ is constant with the lift coefficient, the twist results in a rapidly increasing δ as the lift coefficient decreases. This is true because the basic load distribution due to twist remains unchanged, while the additional load distribution determined by the planform proportionally decreases with the lift coefficient and, since the resultant load distribution is the sum of the two above, at low lift coefficients, the effects of the twist become more and more predominant. While $\delta = 2.5$ per cent at high lift coefficients, it has grown to $\delta = 59$ per cent at $C_L = 0.25$. The control deflection required to trim has an alleviating effect on the induced drag increment due to twist at the lower lift coefficients. The actual conditions are represented by the heavy curve which includes the effect of all influencing facotrs. By reference to this, it can be seen that $\delta = 35$ per cent at $C_{L_{max}}$ and gradually decreases to $\delta = 24$ per cent at $C_L = 0.5$.

Below $C_L = 0.5$, δ increases again, but not nearly so rapidly as in the case of the twisted wing without control deflection.

Parasite Drag

The parasite drag of a flying wing is supposed to be negligible, since the frontal and wetted area of the fuselage are very small compared to the entire wing area. Tuft observations on the Horten IV, however, indicated intense separation on the rear part of the cockpit hatch which implies genesis of considerable parasite drag. Figure 8 shows tuft photographs of the canopy throughout the speed range. As can be seen, the separated region becomes gradually reduced and finally diminished as the speed increases. Figure 9 presents the extent of separation evaluated from tuft photographs. The attitude of the plane as well as the angle of flight path, pitch, and angle of attack are given also. The steep nose up attitude of the canopy at high lift coefficients, which incorporates severe adverse pressure gradients, is apparently the major source of the separation.

Since there is no practical method available for measuring the parasite drag numerically, it is determined indirectly by subtracting the profile and induced drag from the measured total drag. The remainder is considered parasite drag.

Breakdown of the Drag Polar

In Figure 10, the drag polar is divided into the major components discussed in the foregoing paragraphs. The induced drag consists of two parts: the theoretical value, that associated with an elliptic lift distribution; and the increment, due to the actual conditions. The former part being proportional to the square of the lift coefficient, appears in the linearized drag polar as a straight line with a slope determined by the geometric aspect ratio. At the maximum lift coefficient, this part amounts to about 35 per cent of the total drag. The other part, the induced drag increment, progressively increases with the lift coefficient, and at $C_L = 1.00$, results in about 30 per cent higher induced drag than the theoretical. Thus, the total induced drag amounts to about 46 per cent in low speed flight.

The parasite drag is negligible at low lift coefficients, but begins to grow gradually between $C_L = 0.4$, and 0.7. Above $C_L = 0.7$, the separation from the canopy expands rapidly and the parasite drag rises from 3 to 14 per cent of the total.

The profile drag forms a major part of the total drag throughout the entire speed range, and becomes more and more predominant at low lift coefficients. It is 90 per cent at $C_L = 0.2$. It can be seen that the main responsibility for the lower than expected performance rests with the high profile drag and its intense growth with lift coefficient.

On the basis of the Figure 10, the low span efficiency can be explained also. The span efficiency is defined as the ratio between the slopes of the theoretical and actual induced drag polars plotted in linearized form: C_L^2 versus C_D. In other words, it is the ratio of the effective and geometric aspect ratio. Simplified theoretical considerations often assume, however, that the profile and parasite drag are constant, that is, the total drag polar is parallel to the actual induced drag polar. Hence, it is a general practice to express the span efficiency as the ratio between the slopes of the theoretical induced drag polar and the total drag polar. This is, however, not precise, since in practice both the profile and parasite drag are subject to change with the lift coefficient, and the slope of the total drag polar is accordingly different from that of the actual induced drag polar.

In the case of the Horten IV, using the slope of the total drag polar, the span efficiency appears to be 53 per cent, however the actual span efficiency, using the induced drag increment, is 76 per cent.

The Maximum Lift Coefficient

A further weakness of the Horten IV, which was not clearly understood, is the low maximum lift coefficient. This can be cleared also by studying the lift distribution at minimum speed.

In Figure 11, the actual local lift coefficient is plotted along the span for $C_L = 1.125$. The peak value, $c_{l_{max}} = 1.36$, occurs at about 35 per cent of the half span, that is, somewhat inboard of the

elevons. Tuft observations revealed that intense separation exists at the same place when the plane flies at the minimum speed. This means that the stall is initiated there, that is, the local lift coefficient reaches its maximum possible value. Since $c_{l\ max}$ for a given airfoil depends primarily upon the Reynolds number, the maximum available lift coefficient for the rest of the wing can be estimated. Accordingly, $c_{l\ max} \approx 1.4$ for the wing root ($Re = 1.7 \times 10^6$) and $c_{l\ max} \approx 1.00$ for the tip ($Re = 0.4 \times 10^6$). In Figure 11, the maximum available local lift coefficient is also indicated. The difference between this and the curve of actual lift coefficient, designated as lift reserve, indicates the margin of safety against tip stall.

As can be seen, the local lift coefficient reaches the limit of the stall once at the third half span and once more at the outer end of the inboard elevon, but remains far below the limit on the outboard part of the wing due to the highly deflected control surfaces. This implies a great safety margin against tip stalling, but simultaneously results in a considerable loss in lift. This is why the resultant maximum lift coefficient, $C_{L_{max}} = 1.125$, is so low although the airfoil itself has a normal $c_{l_{max}} = 1.3$ to 1.4, at the Reynolds numbers concerned. For comparison, the lift coefficient distribution for the wing without control deflection is given also in Figure 11. This shows that the local lift coefficient would exceed the available limit over the outer portion of the wing, resulting in tip stall. Consequently, some negative control deflection at the tips is necessary, however much less would be sufficient to provide favorable stall characteristics than actually is applied.

Possible Performance Improvements

On the basis of the foregoing drag analysis, the possibilities of performance improvement will be discussed below. This is based on a calculation in which we assumed several successive improvements in the drag components, which are believed reasonable in the present state of development. These improvements are the following:

1. A reduction of the profile drag to the level of the present laminar airfoils. For comparison, the profile drag polars of the Horten IV and the Phoenix are presented in Figure 12. Also, two imaginary polars for the Horten IV, used in the present calculation, are shown. One of severely increasing drag, like the original; another, which has nearly constant drag up to $C_L = 0.8$. The latter could be achieved only if the extent of the elevon surfaces, or their deflection providing the trim, were greatly reduced by some means.

2. The induced drag increment, which is 25 to 30 per cent, could be reduced to at least 8 to 10 per cent if the excessive twist and large negative control deflection were reduced. Variable sweep, C. G. position, or twist might be a solution to this problem.

3. The parasite drag is considered completely eliminative by providing a separation-free pilot compartment.

Figure 13 demonstrates the result of these improvements on the gliding performance. Curve No. 1 is the present state; Nos. 2, 3, and 4, show the performance if only one of the three drag components were improved at one time. Thus, the importance of the several modifications can be seen clearly. Namely, the complete elimination of the parasite drag would affect the performance mostly at low speeds, and the best gliding ratio would be barely increased. (Curve No. 2). The reduction of the induced drag increment to 10 per cent would increase the best gliding ratio from 29.5 to 32 only. (Curve No. 3). But a considerable improvement follows when the profile drag is reduced. Curve No. 4 was obtained by using the imaginary profile drag polar marked as "A" in Figure 12. The best gliding ratio rises to 40, and the performance at high speed, that is, the penetration ability, is greatly increased. Curves No. 5 and 6 show the improvement, if in addition to the above profile drag reduction, the parasite drag were eliminated and the induced drag were decreased in the formerly described manner. In this case, a remarkable improvement appears in the low speed region, and the best gliding ratio becomes 41.5 and 43.5 respectively. Finally, the Curve No. 7 represents the ultimate performance which could be achieved with the other imaginary profile drag polar marked "B" in Figure 12, naturally assuming the above mentioned

improvements in induced and parasite drag. In this case, the best gliding ratio would be 48, a really phenomenal one.

Conclusions

The present investigation has basically cleared the conditions by which the performance of the Horten IV was limited. However, a large margin of improvement seems to be possible by means of proper drag reduction. An up-to-date flying wing of the size of the Horten IV should be able to reach a best gliding ratio of nearly 50 to 1. In the case of one of the very best conventional designs, like the Phoenix, such a high performance seems to be feasible only if estensive boundary layer control were applied. This verifies that the flying wing design is not an obsolete idea, but is worthy of further development.

It is beyond the scope of this paper to deal with the stability and control characteristics in detail, nevertheless, the author wishes to note that, in his opinion, the handling of the Horten IV is not essentially more difficult than that of any other high performance sailplane. The extremely good natured stalling and circling characteristics, as well as the excellent landing maneuverability are to be noted especially. The prone position of the pilot is believed to provide a more natural sensation of flight than the conventional sitting position; in addition, it provides uncomparable visibility for landing and navigation. On the other side of the balance, however, the marginal directional stability, unusual response for rudder control coupled with pitch, and above all, the wing tip flutter, appearing above 140 km/h., should be noted.

Drawing the final conclusions, we summarize once more the major deficiencies of the Horten IV and outline the possible ways of improvement in Table II.

Two of the suggested improvements are of primary importance, that is, the use of a low drag laminar airfoil and the elimination of large control deflection by some means, for example, by variable sweep or center of gravity. The variable sweep seems to be fairly practical, however, a more detailed consideration is necessary to find out which would be the more favorable way. To do this, of course, the stability and control characteristics are to be taken into consideration also.

Since the keystone of the performance improvement lies in the use of a laminar airfoil, this, in case of the Horten IV, would mean a complete reconstruction of the airframe. Therefore, further development seems more reasonable through a new design, in which all the experiences gained so far as well as the latest technology of construction could be utilized.

This does not mean, however, that there is nothing to do with the Horten IV as far as further research is concerned. Namely, for the sake of further development it would be badly needed to evaluate the stability and control characteristics, similarly as was done for the performance. Moreover, it would be very useful to make an experiment on variable sweep, before adopting it for a new design and the Horten IV seems to be suitable for this experiment.

We, at Mississippi State University, have planned to continue this work through further evaluation and study toward a new flying wing design, in which the brave old Horten IV would be reincarnated. The tragic death of Dr. August Raspet, who was the leading spirit in this aspiration, however, has made the chances of realizing this plan very uncertain.

TABLE I

MEASURED AERODYNAMIC AND PERFORMANCE DATA

	DFS*	MSU*
$C_{D_{min}}$	0.01175	0.0125
$C_{L_{max}}$	1.17	1.125
$\frac{dC_L}{d\alpha}$ Rad^{-1}	—	4.35
$\frac{C_{L\,max}}{C_{D\,min}}$	99.5	90
$\varepsilon_{max} = (\frac{L}{D})_{max}$	31.5	29.5
e	63%	53%
λ_{eff}	13.4	11.3
v_{min} m/sec	0.59	0.70
$V_{w_{min}}$ km/h	60.	70.
V_{min} km/h	52.	59.5
$V_{\varepsilon_{max}}$ km/h	76.	82.
$V_{\varepsilon = 20}$ km/h	130.	126.

* Data reduced from DFS actual tested gross weight W=325 kg. to W=366 kg. C. G. position is unknown.

**Acutal tested gross weight W=366 kg. C. G. position 1.38 meters from the nose point (See Figure 5).

TABLE II

SUMMARY OF THE EVALUATION OF HORTEN IV

CONCERNING THE PERFORMANCE

Deficiency	Reason	Possible Way of Improvement
High profile drag	1. Obsolete airfoil	Use of laminar airfoil
	2. Disturbance of the airfoil by control surfaces, dive brakes and drag rudders	Smaller but more effective control surfaces with sealed gap. Different arrangement of dive brakes and rudders.
	3. Excessive control deflection	Variable sweep or C. G. to provide trim
	4. Low Reynolds number at the tip due to high taper ratio	Moderate taper ratio
High induced drag	Excessive twist control deflection, and taper	Variable sweep or C. G. to provide trim, less taper
High parasite drag	Separation from the canopy	Different canopy arrangement
Low maximum lift coefficient	Excessive control deflection, excessive taper	Variable sweep or C. G. and, perhaps, variable twist, less taper

REFERENCES

1. Wilkinson, K. G., : "The Horten Tailless Aircrafts," RAE Rep FA 259/1, T. N. No. Aero 1703, October, 1945.

2. Zacher, Hans,: Ergebnisse der Leistungmessung und Flugeigenschaft prüfung des Segelfugzeuges D-30 "Cirrus." Mitteilungen der Flugtechnischen Fachgruppen and Arbeitgemeinschaften, Folge 6/September 1944.

3. Machin, K. E.: The Performance Testing of the Slingsby Sky," Journal of the Royal Aeronautical Society, July, 1954.

4. Raspet, A.: "Leistungsteigerung von Segelflugzeugen durch die Berücksichtigung der Grenzschichtforschung." Hirth, W.: Handbuch des Segelfliegens 125/145 pp.

5. Silverstein, A., and Katzoff, S.: "Simplified Method for Determining Wing Profile Drag in Flight." Journal of Aeronautical Sciences, Vol. 7, No. 7, 1940, 295/301 pp.

6. Raspet, A.: "Boundary Layer Studies in a Sailplane," Aeronautical Engineering Review, June 1952, 52/60 pp.

7. Schrenk, O.: "A Simple Approximation Method for Obtaining the Spanwise Lift Distribution," NACA TM948, 1940.

8. Weissinger, J.: "The Lift Distribution of Swept-Back Wings," NACA TM 1120, 1947.

9. Rácz, E.: Airplane Design, Tankönyvkiadó, Budapest, 1955.

10. Gruber, J., Blahó, M.: Fluid Mechanics, Tanönyvkiadó, Budapest, 1956.

Figure 1

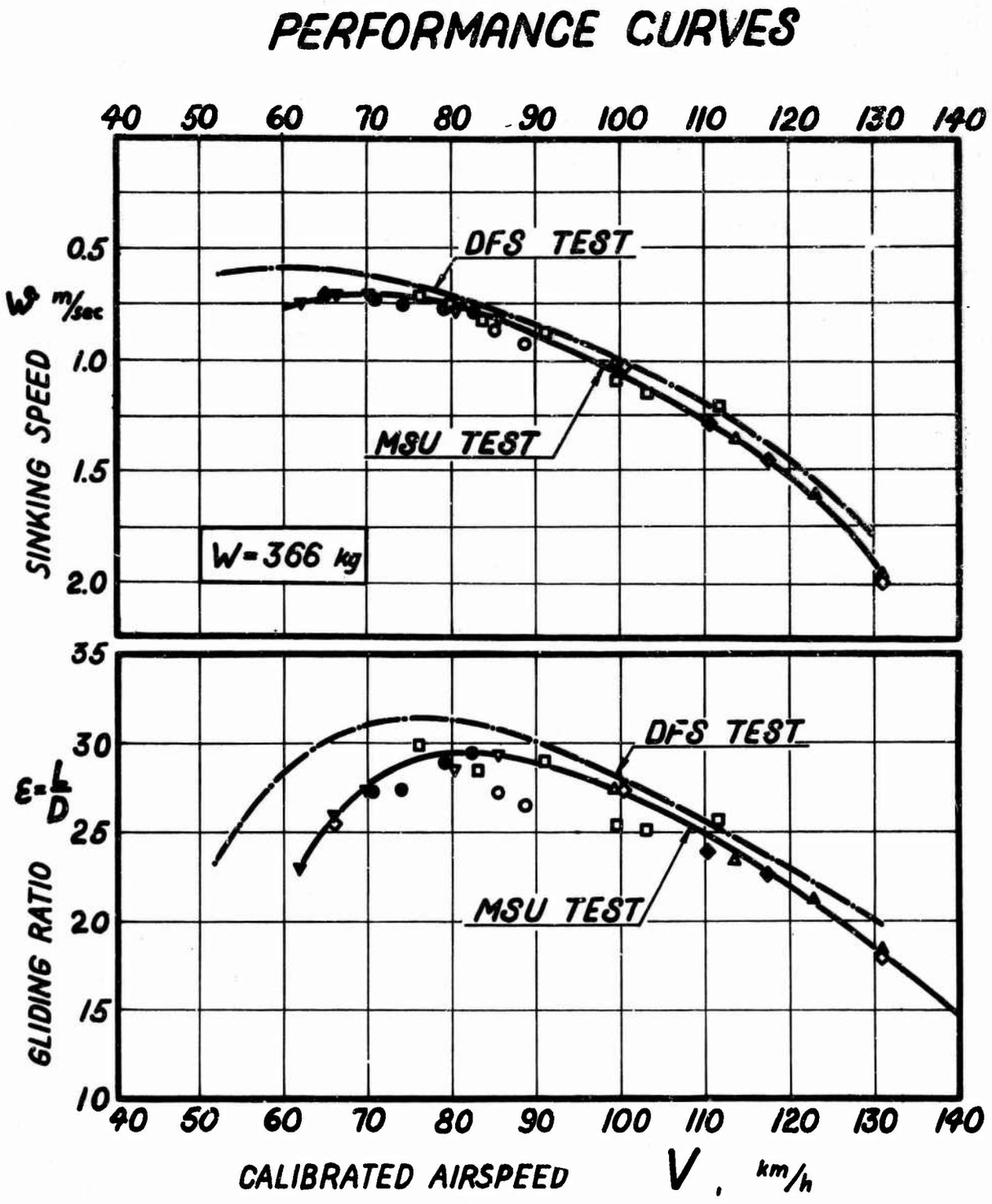
PERFORMANCE CURVES
40 50 60 70 80 90 100 110 120 130 140
0.5
1.0
1.5
2.0
w m/sec
SINKING SPEED
DFS TEST
MSU TEST
W=366 kg
35
30
25
20
15
10
ε=L/D
GLIDING RATIO
DFS TEST
MSU TEST
40 50 60 70 80 90 100 110 120 130 140
CALIBRATED AIRSPEED V, km/h

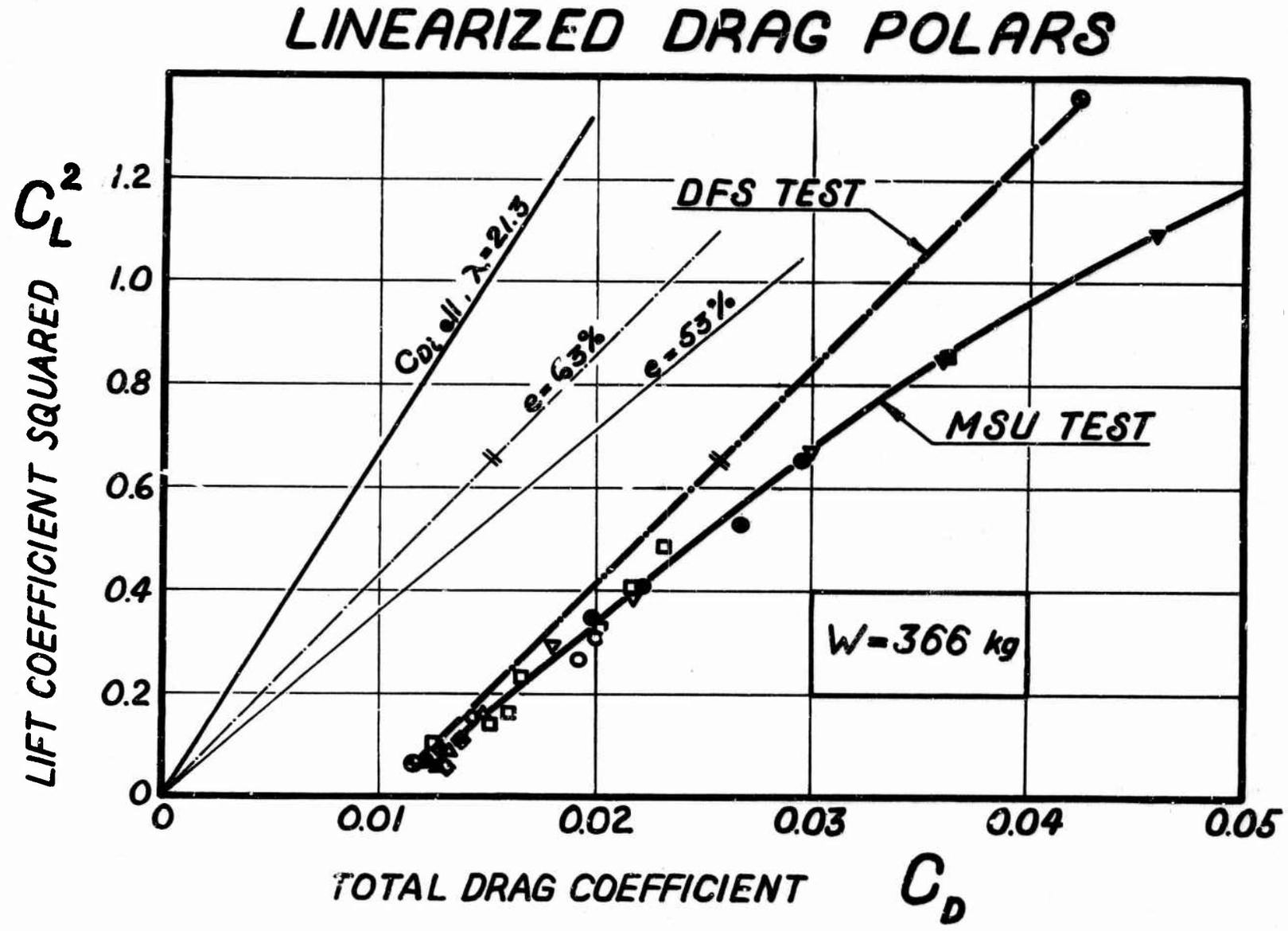
LINEARIZED DRAG POLARS
LIFT COEFFICIENT SQUARED C_L^2
1.2
1.0
0.8
0.6
0.4
0.2
0
0
0.01
0.02
0.03
0.04
0.05
TOTAL DRAG COEFFICIENT C_D
C_{D_i} ell, λ=21.3
e=63%
e=53%
DFS TEST
MSU TEST
W=366 kg

Figure 2

Figure 3

LOCAL PROFILE DRAG POLARS

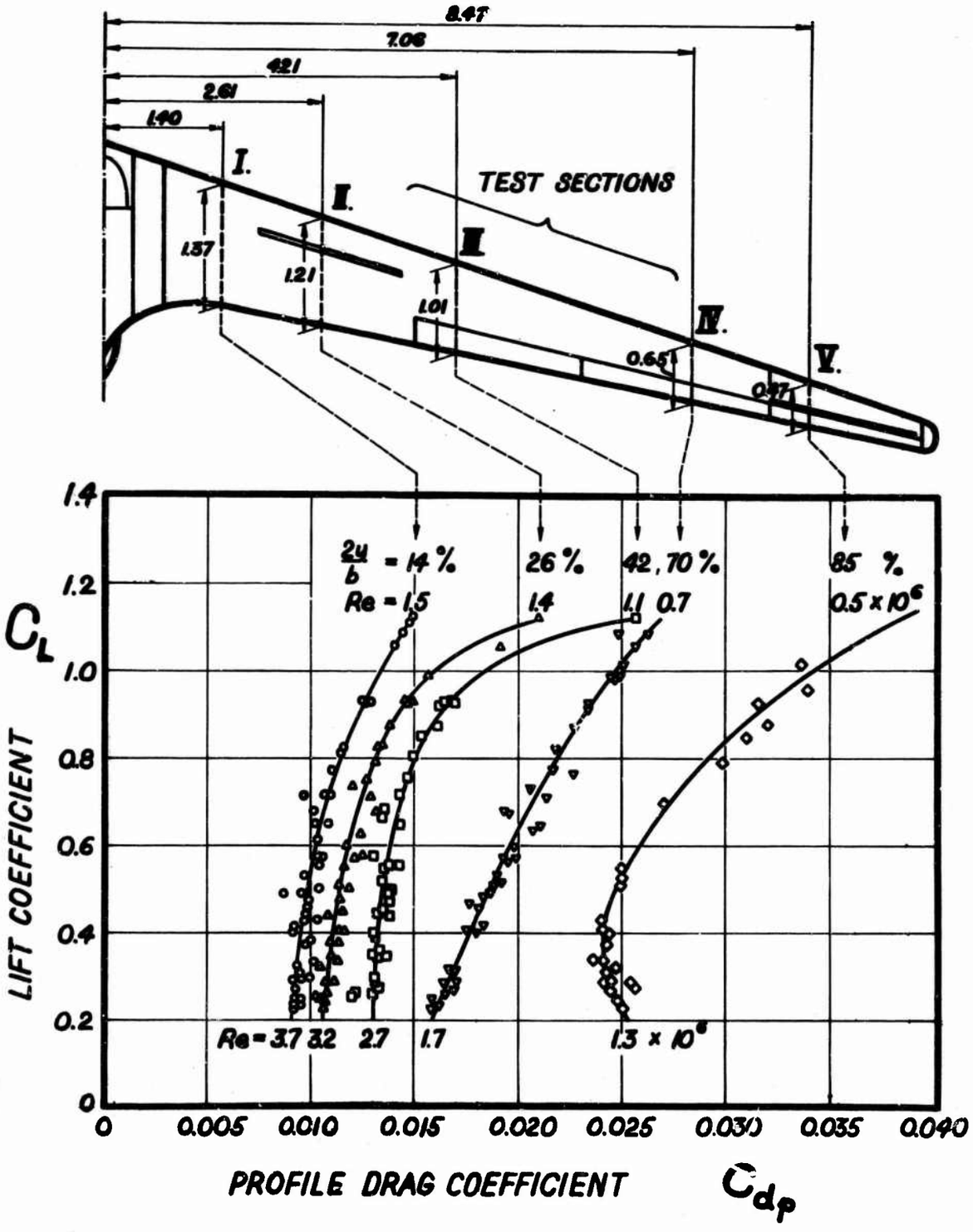

Figure 4

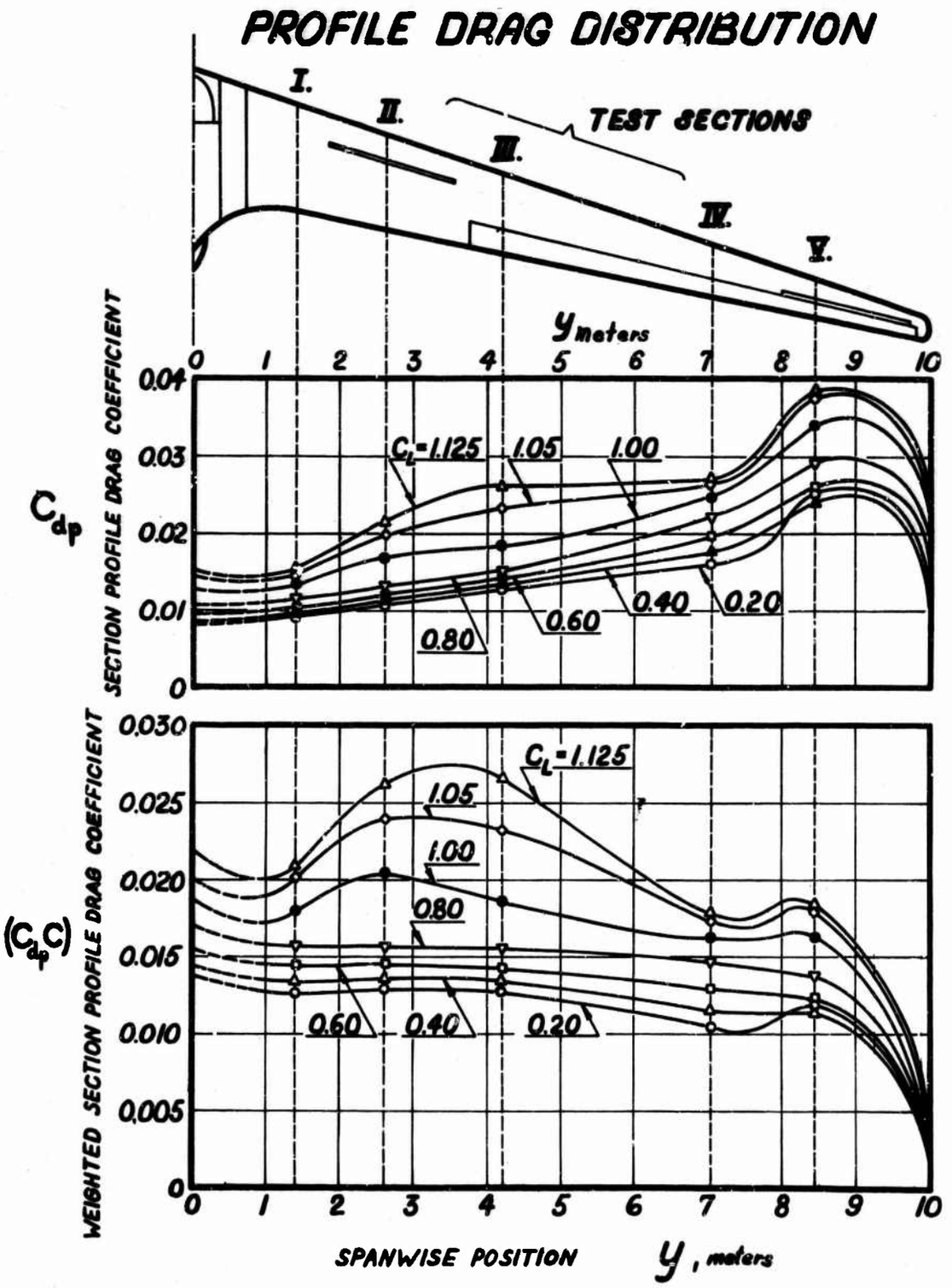
PROFILE DRAG DISTRIBUTION
I.
II.
III.
IV.
V.
TEST SECTIONS
y meters
0 1 2 3 4 5 6 7 8 9 10
C_{dp}
SECTION PROFILE DRAG COEFFICIENT
0.04
0.03
0.02
0.01
0
C_l = 1.125
1.05
1.00
0.80
0.60
0.40
0.20
(C_dC)
WEIGHTED SECTION PROFILE DRAG COEFFICIENT
0.030
0.025
0.020
0.015
0.010
0.005
0
C_l = 1.125
1.05
1.00
0.80
0.60
0.40
0.20
0 1 2 3 4 5 6 7 8 9 10
SPANWISE POSITION y, meters

Figure 5

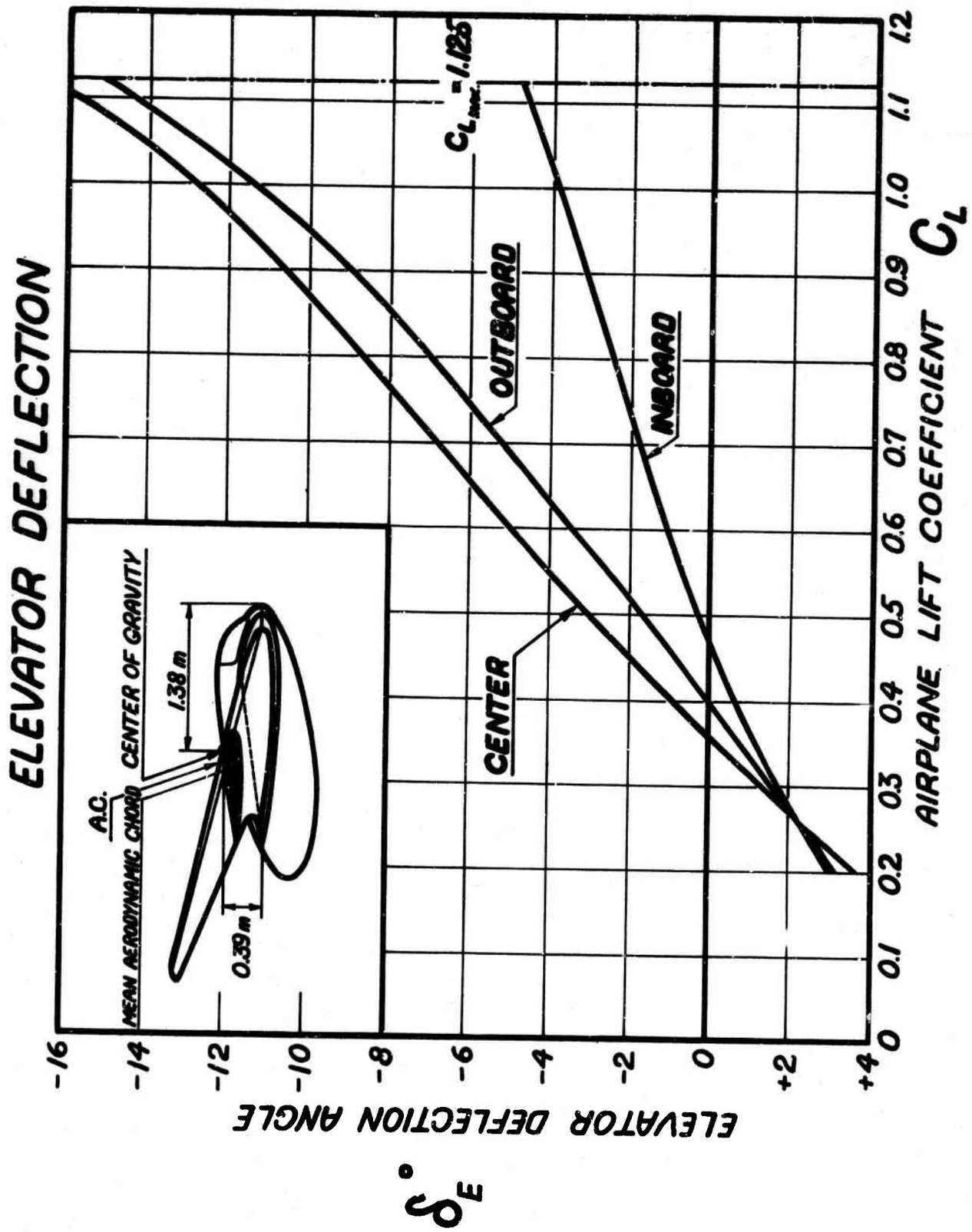
ELEVATOR DEFLECTION
AIRPLANE LIFT COEFFICIENT C_L
ELEVATOR DEFLECTION ANGLE δ_E°
$C_{L_{MAX.}}$ = 1.125
OUTBOARD
INBOARD
CENTER
A.C.
MEAN AERODYNAMIC CHORD
CENTER OF GRAVITY
1.38 m
0.39 m
-16
-14
-12
-10
-8
-6
-4
-2
0
+2
+4
0
0.1
0.2
0.3
0.4
0.5
0.6
0.7
0.8
0.9
1.0
1.1
1.2

Figure 6

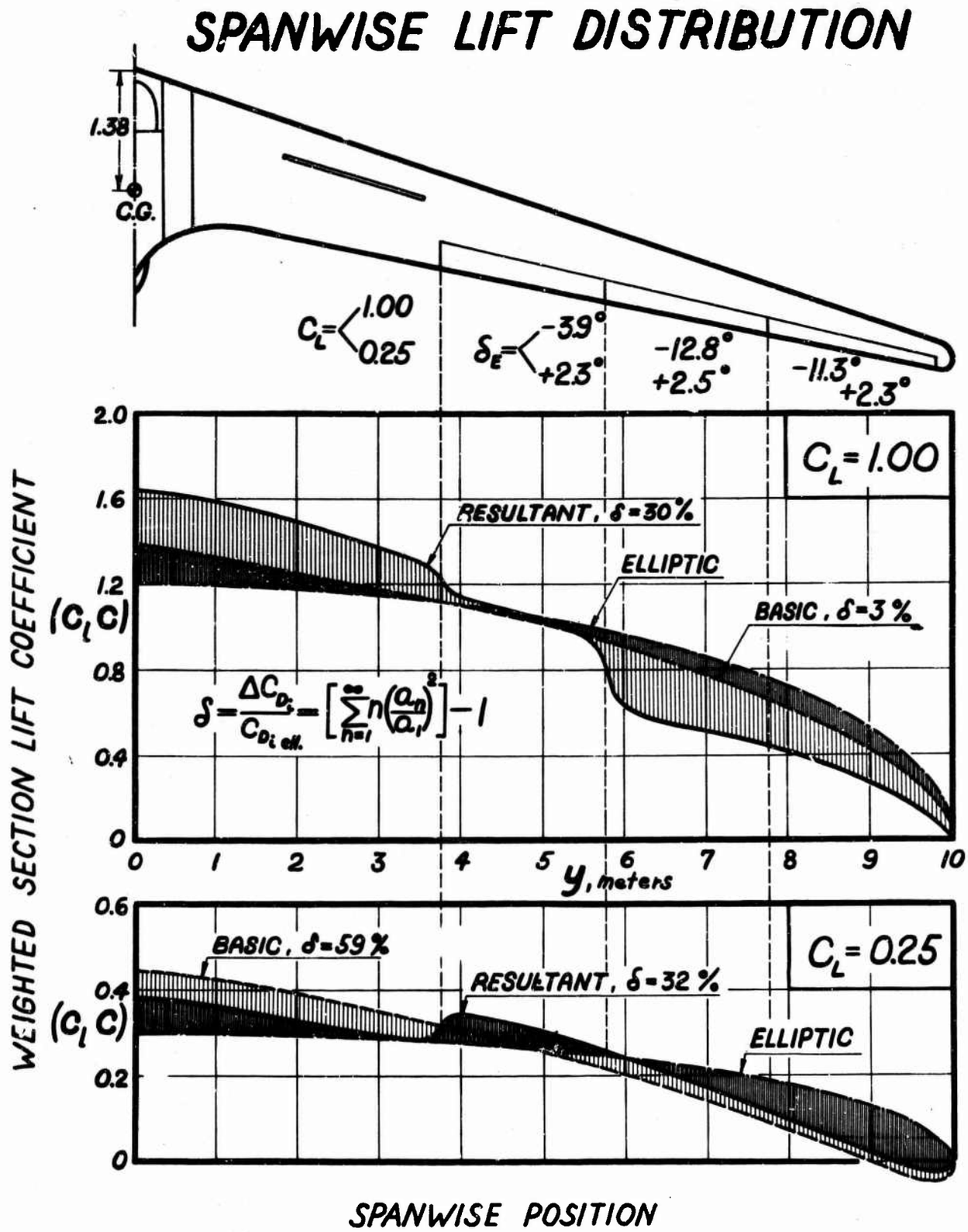
SPANWISE LIFT DISTRIBUTION
1.38
C.G.
C_L = 1.00 / 0.25
δ_e = -3.9° +2.3° / -12.8° +2.5° / -11.3° +2.3°
C_L = 1.00
RESULTANT, δ = 30%
ELLIPTIC
BASIC, δ = 3%
$\delta = \frac{\Delta C_{D_i}}{C_{D_{i\,ell.}}} = \left[\sum_{n=1}^{\infty} n\left(\frac{a_n}{a_1}\right)^2\right] - 1$
C_L = 0.25
BASIC, δ = 59%
RESULTANT, δ = 32%
ELLIPTIC
WEIGHTED SECTION LIFT COEFFICIENT
$(C_l C)$
y, meters
SPANWISE POSITION

Figure 7

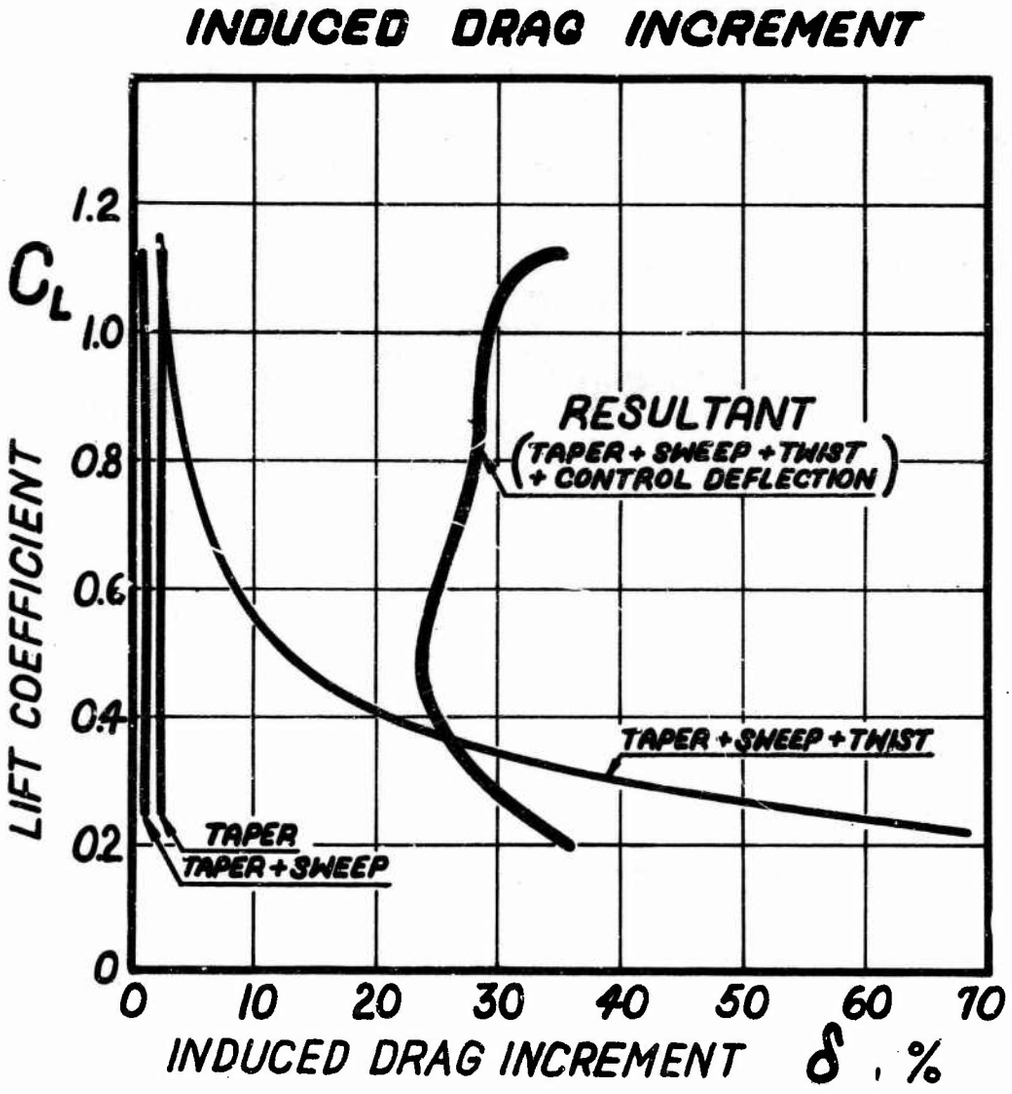
INDUCED DRAG INCREMENT
LIFT COEFFICIENT C_L
1.2
1.0
0.8
0.6
0.4
0.2
0
RESULTANT
(TAPER + SWEEP + TWIST
+ CONTROL DEFLECTION)
TAPER + SWEEP + TWIST
TAPER
TAPER + SWEEP
0
10
20
30
40
50
60
70
INDUCED DRAG INCREMENT δ, %

Figure 8 Tuft Photographs

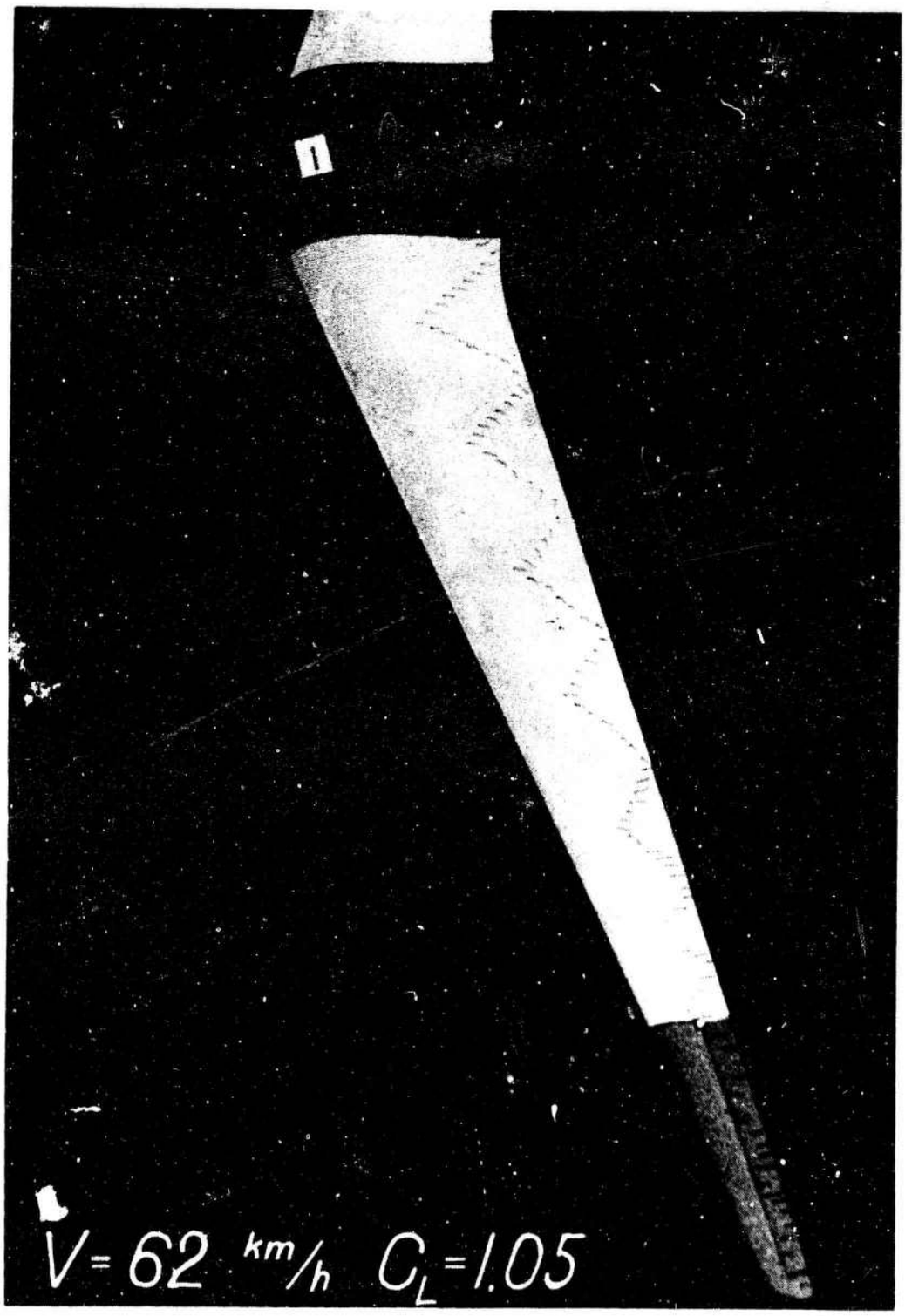

Figure 8 Continued

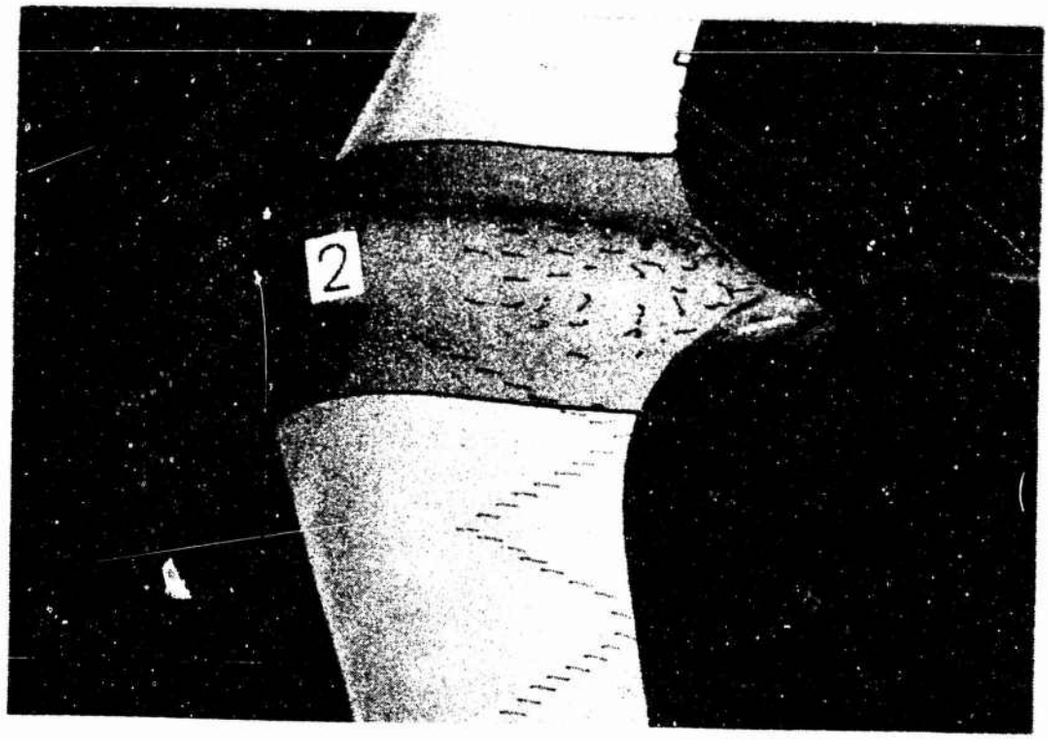

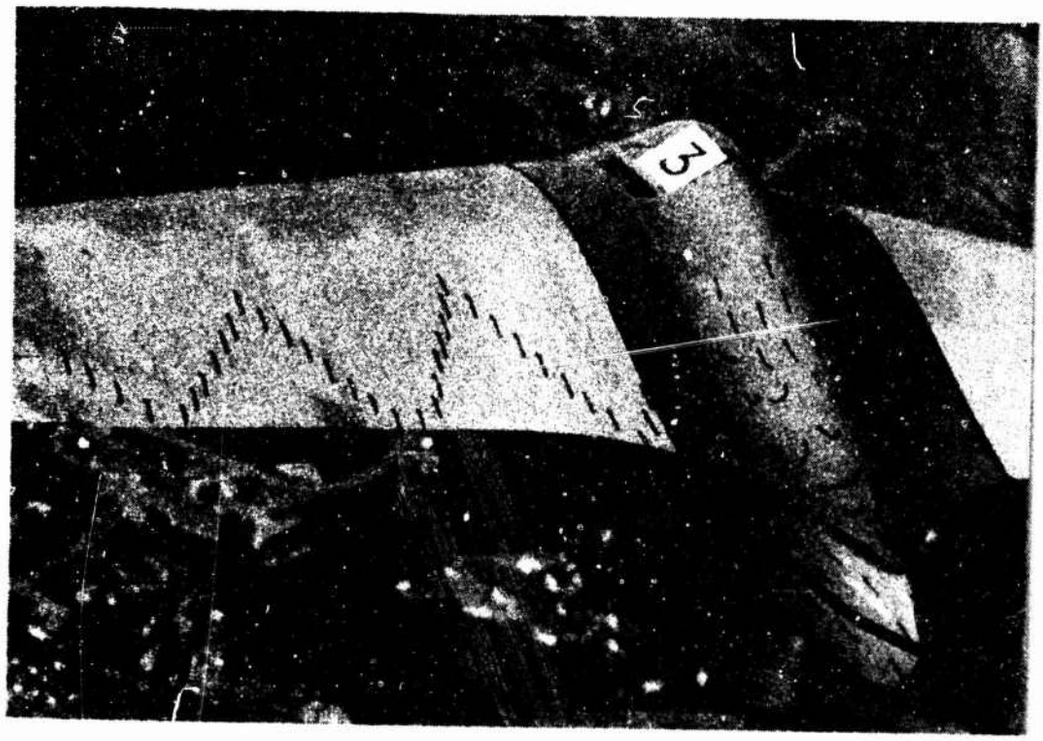

Figure 8 Continued

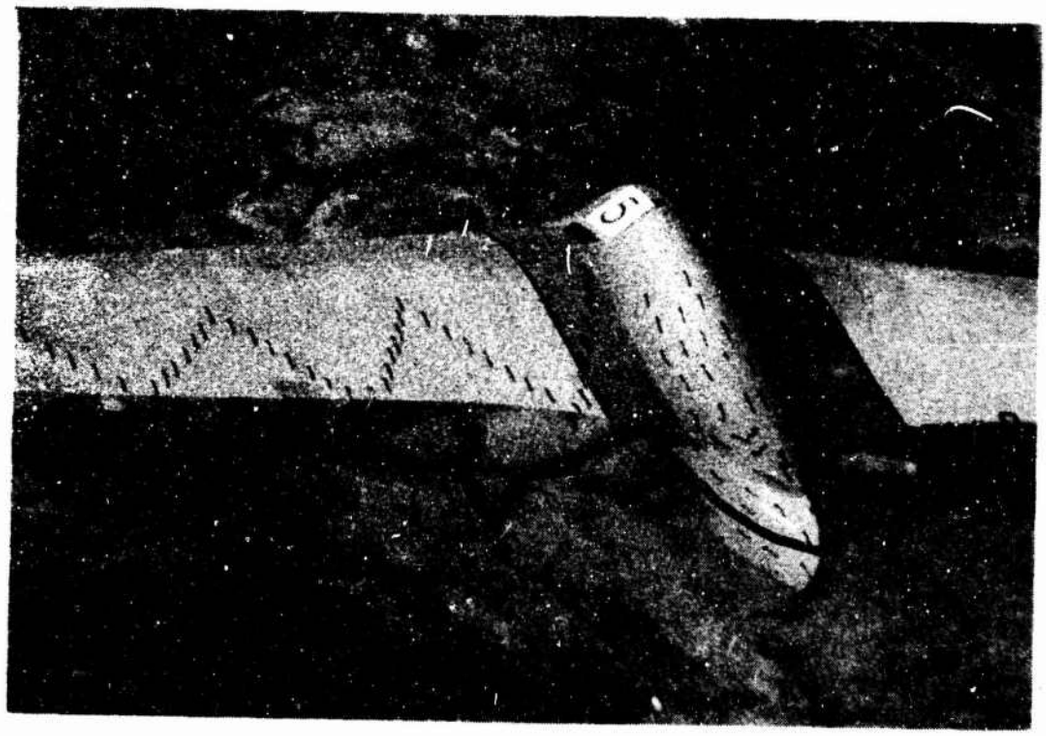

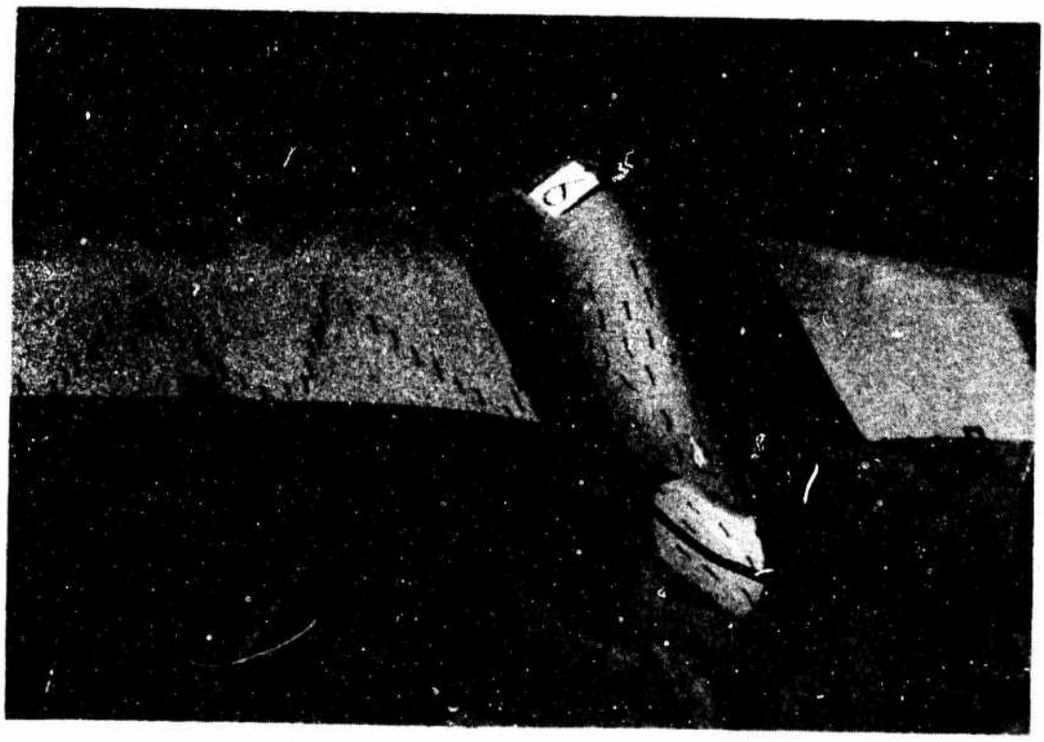

Figure 8 Continued

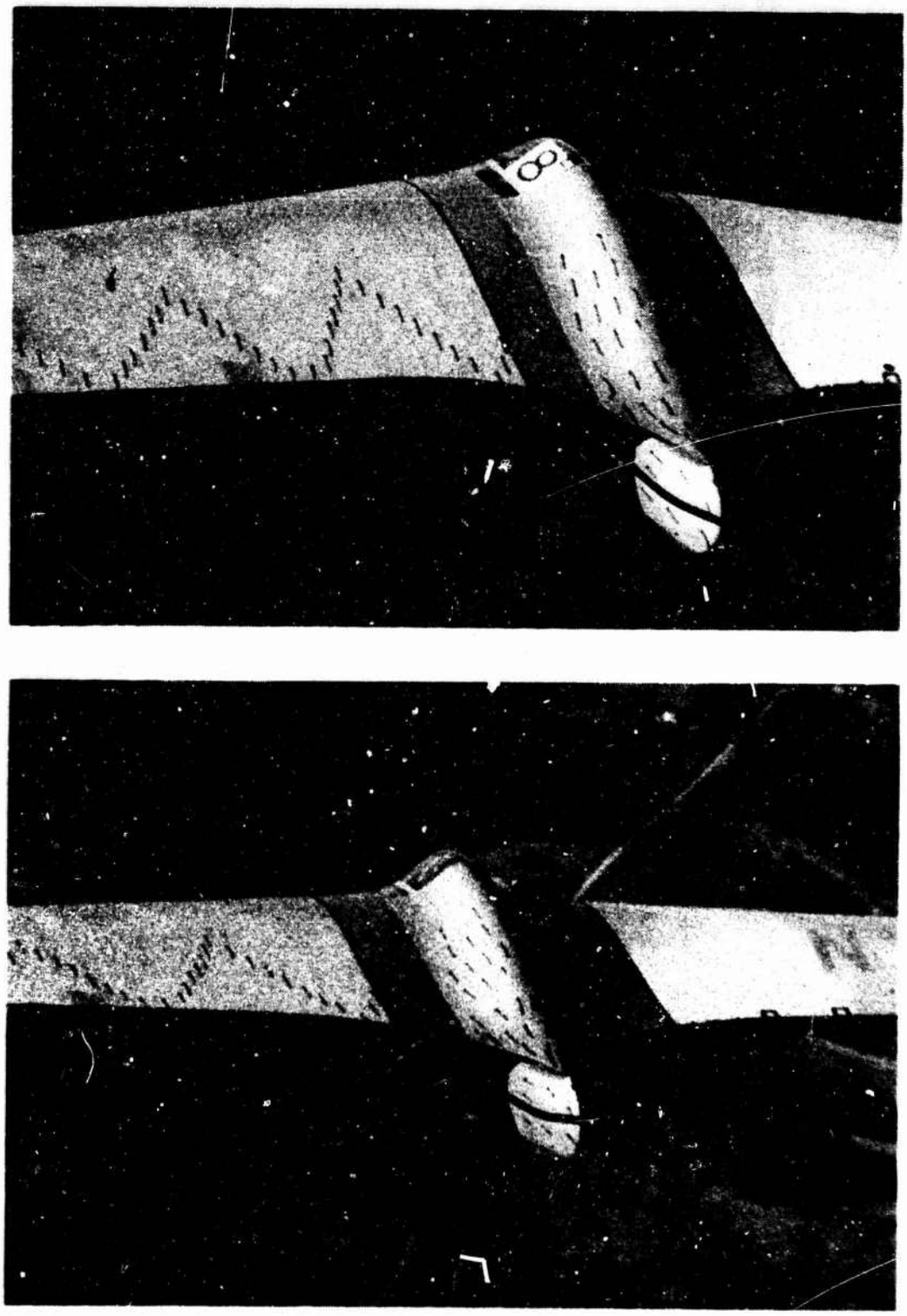

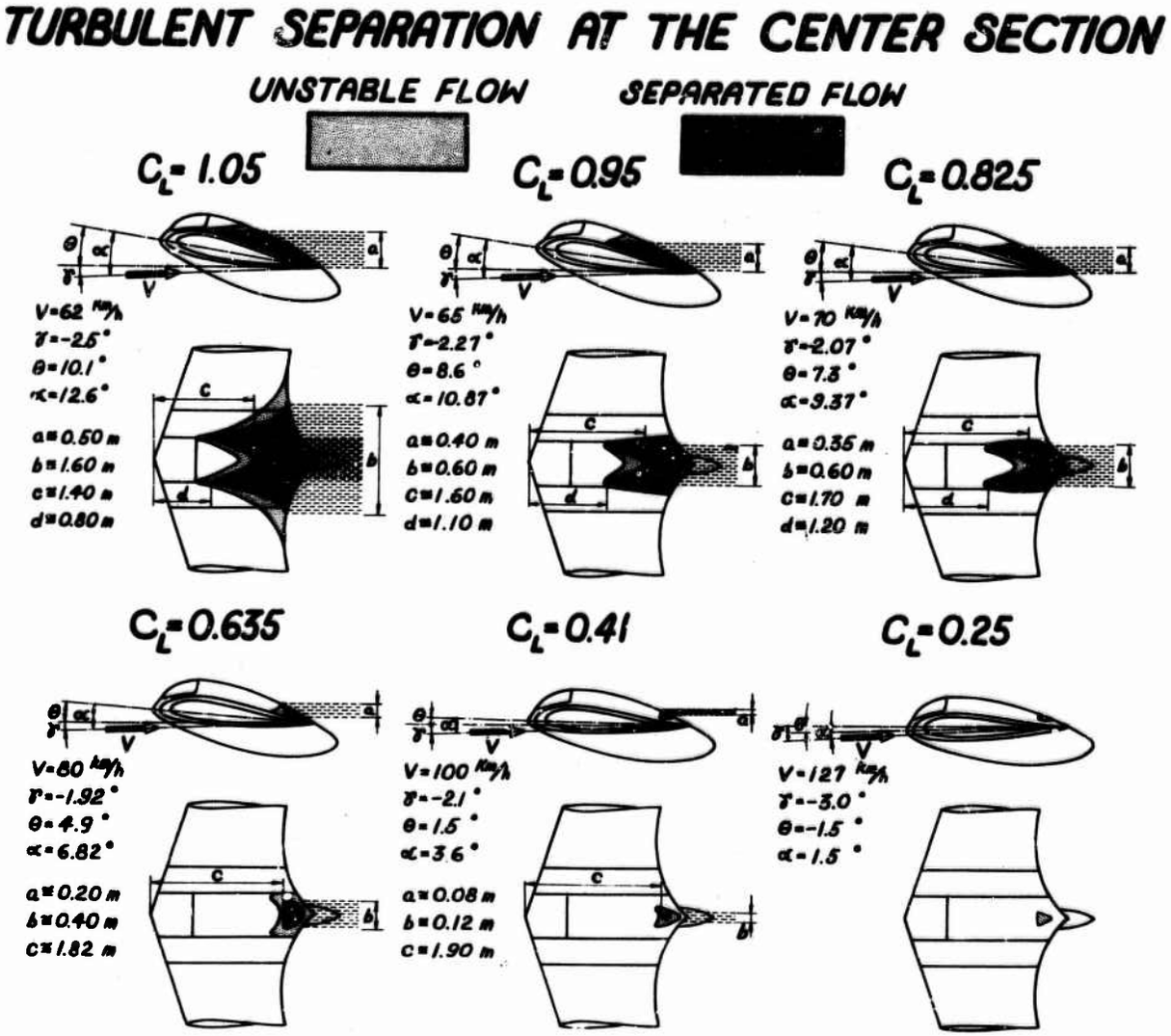
TURBULENT SEPARATION AT THE CENTER SECTION
UNSTABLE FLOW
SEPARATED FLOW
C_L= 1.05
V=62 Km/h
γ=-2.5°
θ=10.1°
α=12.6°
a=0.50 m
b=1.60 m
c=1.40 m
d=0.80 m
C_L=0.95
V=65 Km/h
γ=-2.27°
θ=8.6°
α=10.87°
a=0.40 m
b=0.60 m
c=1.60 m
d=1.10 m
C_L=0.825
V=70 Km/h
γ=-2.07°
θ=7.3°
α=9.37°
a=0.35 m
b=0.60 m
c=1.70 m
d=1.20 m
C_L=0.635
V=80 Km/h
γ=-1.92°
θ=4.9°
α=6.82°
a=0.20 m
b=0.40 m
c=1.82 m
C_L=0.41
V=100 Km/h
γ=-2.1°
θ=1.5°
α=3.6°
a=0.08 m
b=0.12 m
c=1.90 m
C_L=0.25
V=127 Km/h
γ=-3.0°
θ=-1.5°
α=1.5°

Figure 9

Figure 10

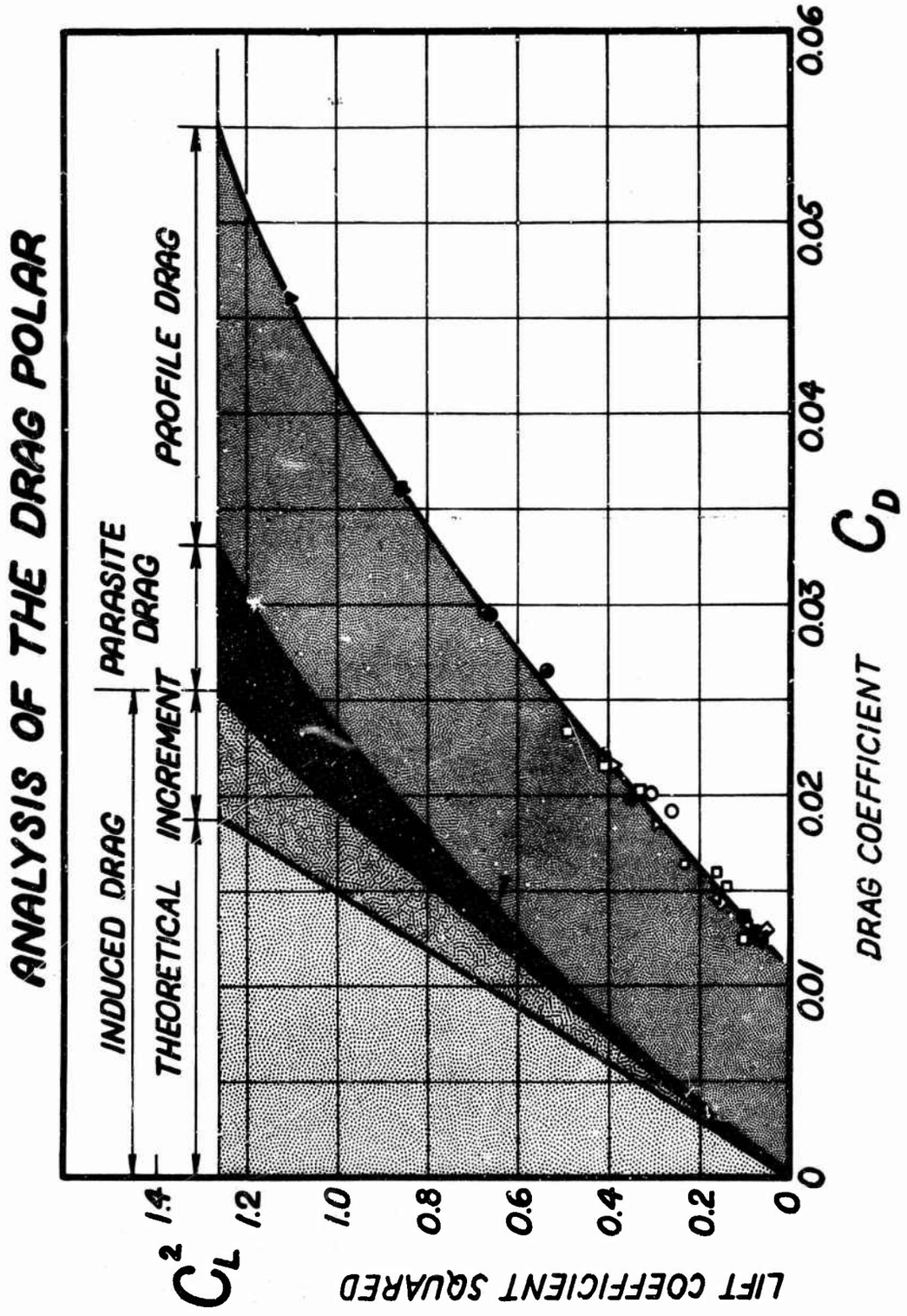
ANALYSIS OF THE DRAG POLAR
INDUCED DRAG
PARASITE DRAG
THEORETICAL INCREMENT
PROFILE DRAG
LIFT COEFFICIENT SQUARED
C_L^2
0
0.2
0.4
0.6
0.8
1.0
1.2
1.4
0
0.01
0.02
0.03
0.04
0.05
0.06
DRAG COEFFICIENT
C_D

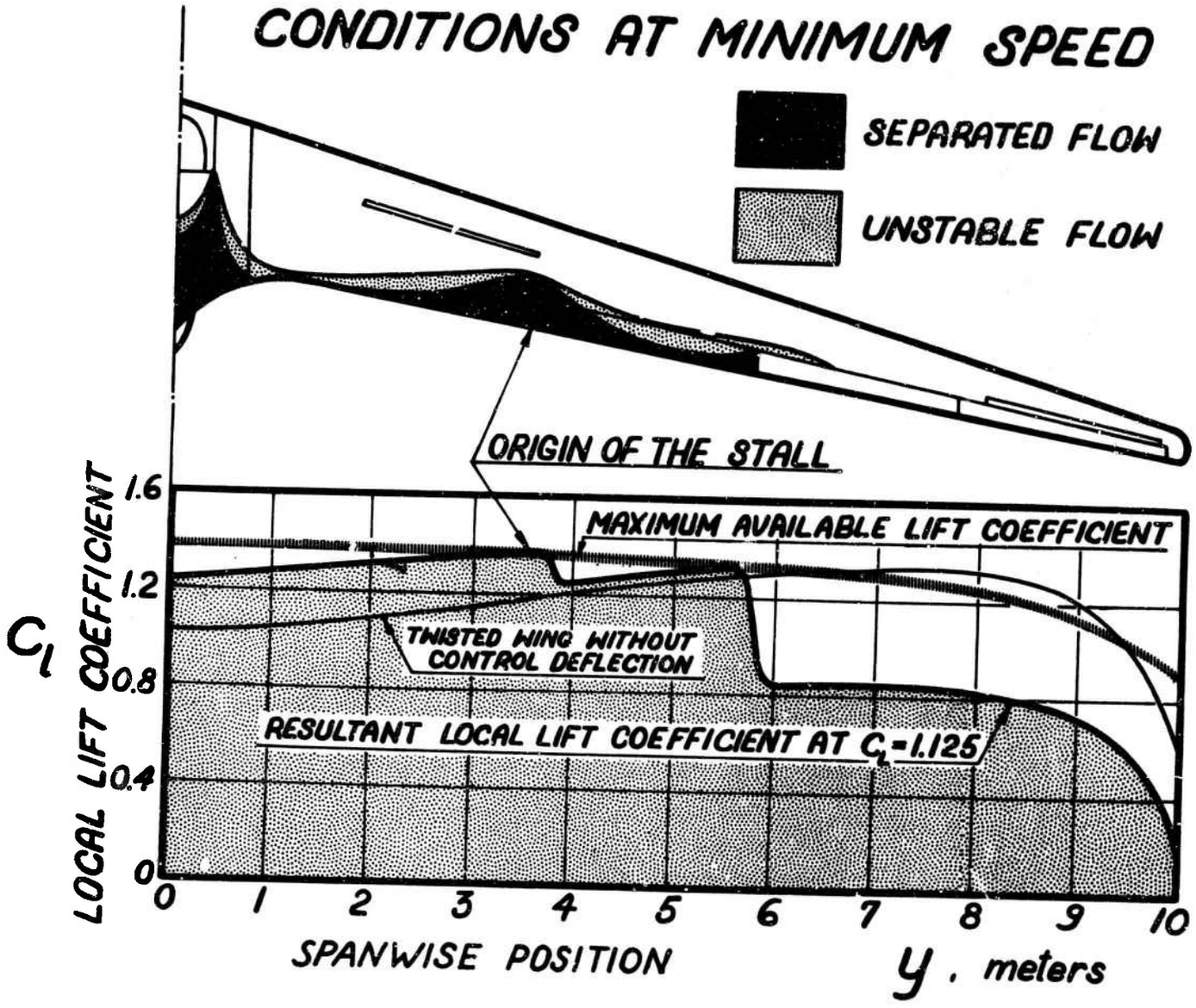
CONDITIONS AT MINIMUM SPEED
SEPARATED FLOW
UNSTABLE FLOW
ORIGIN OF THE STALL
MAXIMUM AVAILABLE LIFT COEFFICIENT
TWISTED WING WITHOUT CONTROL DEFLECTION
RESULTANT LOCAL LIFT COEFFICIENT AT C_L=1.125
c_l LOCAL LIFT COEFFICIENT
1.6
1.2
0.8
0.4
0
0 1 2 3 4 5 6 7 8 9 10
SPANWISE POSITION
y . meters

Figure 11

Figure 12

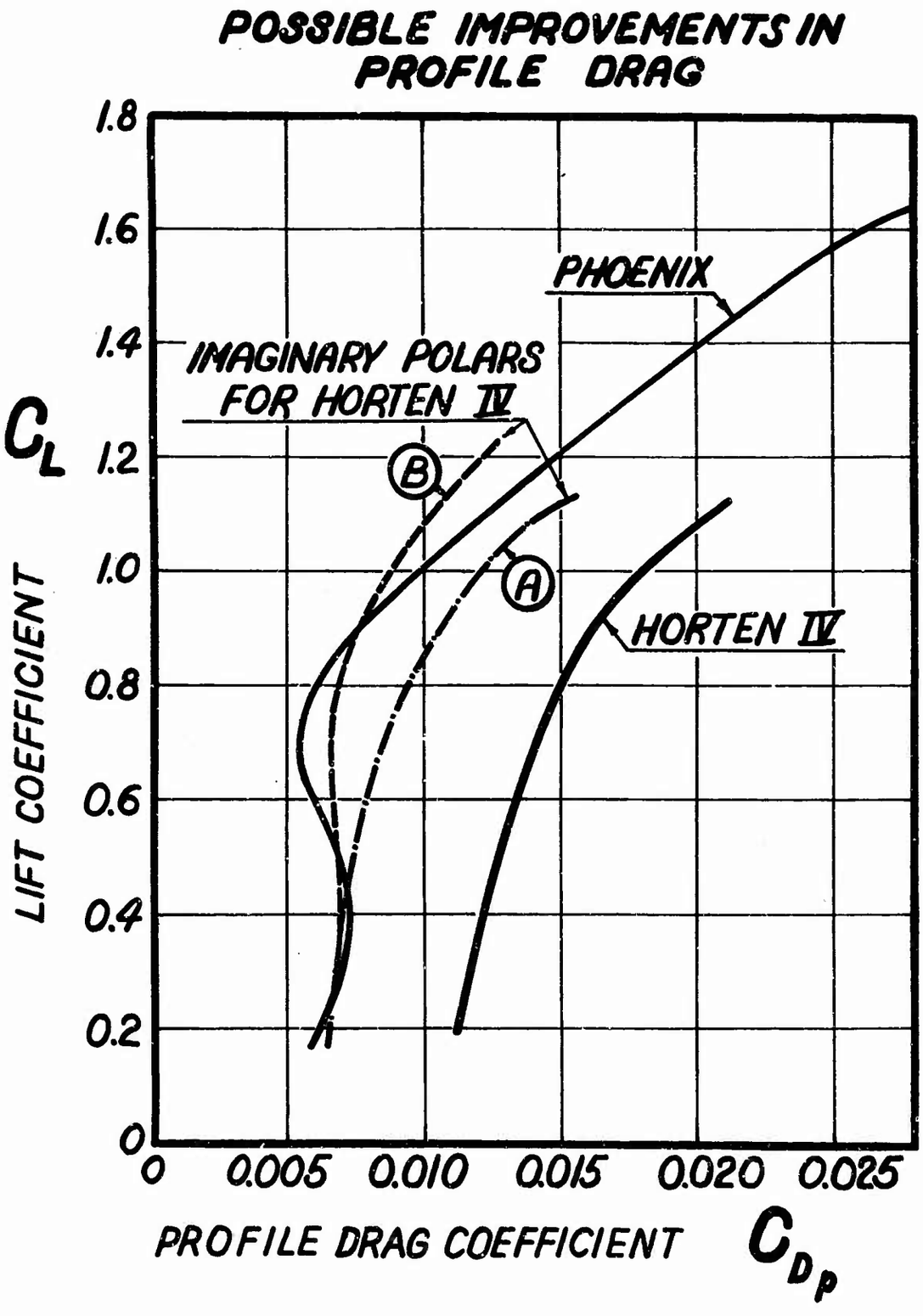
POSSIBLE IMPROVEMENTS IN PROFILE DRAG
1.8
1.6
1.4
1.2
1.0
0.8
0.6
0.4
0.2
0
C_L
LIFT COEFFICIENT
PHOENIX
IMAGINARY POLARS FOR HORTEN IV
B
A
HORTEN IV
0
0.005
0.010
0.015
0.020
0.025
PROFILE DRAG COEFFICIENT
C_{D_p}

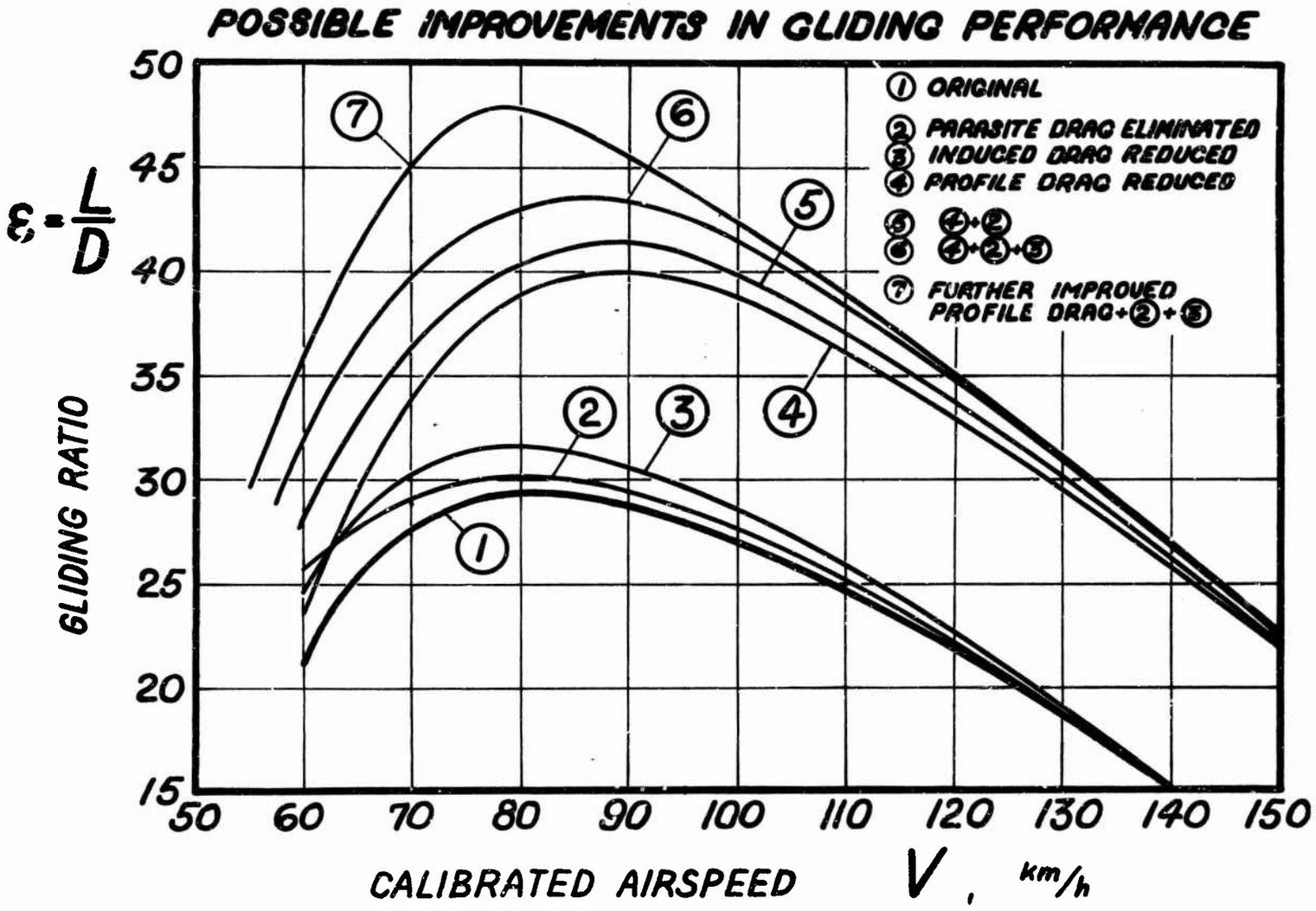
POSSIBLE IMPROVEMENTS IN GLIDING PERFORMANCE
GLIDING RATIO
$\varepsilon = \frac{L}{D}$
50
45
40
35
30
25
20
15
50
60
70
80
90
100
110
120
130
140
150
CALIBRATED AIRSPEED
V, km/h
① ORIGINAL
② PARASITE DRAG ELIMINATED
③ INDUCED DRAG REDUCED
④ PROFILE DRAG REDUCED
⑤ ④+②
⑥ ④+②+③
⑦ FURTHER IMPROVED PROFILE DRAG+②+③
①
②
③
④
⑤
⑥
⑦

Figure 13